J Mater Sci: Mater Med (2011) 22:41–50
DOI 10.1007/s10856-010-4188-0

Corrosion characteristics of anodized Ti–(10–40wt%)Hf alloys for metallic biomaterials use

Yong-Hoon Jeong · Han-Cheol Choe · William A. Brantley

Received: 19 July 2010 / Accepted: 10 November 2010 / Published online: 21 November 2010

Abstract The effect of anodizing on corrosion resistance of Ti–*x*Hf alloys has been investigated. Ti–*x*Hf alloys were prepared and anodized at 120, 170 and 220 V in 1 M H_3PO_4 solution, and crystallized at 300 and 500°C. Corrosion experiments were carried out using a potentiostat in 0.15 M NaCl solution at 36.5 ± 1°C. The Ti–*x*Hf alloys exhibited the α' and anatase phases. The pore size on the anodized surface increases as the applied voltage is increased, whereas the pore size decreases as the Hf content is increased. The anodized Ti–*x*Hf alloys exhibited better corrosion resistance than non-anodized Ti–*x*Hf alloys.

1 Introduction

Pure titanium and titanium alloys are widely used to replace failed hard tissues such as artificial hips, and shoulder and knee joint, as well as dental implants, due to their excellent specific strength, corrosion resistance and biocompatibility. The currently used CP (commercially pure) titanium and the Ti–6Al–4V alloy do not have sufficient strength for some clinical applications. Moreover, when titanium alloys are used in dental applications, elements that are incorporated in titanium should not adversely affect its corrosion behavior in the oral environment [1–3]. However, in the case of the Ti–6Al–4V alloy, the dissolution of vanadium ions from the implant surface have been known to cause serious health problems and adverse tissue reactions [4], while the aluminum ions have been associated with potential neurological disorders [5, 6]. In addition, long-term experiences indicate that the Ti–6Al–4V alloy transfers insufficient load to the adjacent remodeling bone, which may result in bone resorption and eventual loosening of the prosthetic devices [5, 7]. In order to overcome these disadvantages and to achieve better performance in terms of mechanical properties and biocompatibility, new Ti alloys containing non-toxic and non-allergic secondary elements such as Nb, Ta, Zr, Hf, Mo, and Sn have been developed [8–12]. The element hafnium belongs to the same group as that of titanium in the periodic table; hence an alloy of titanium with hafnium would be expected to demonstrate good corrosion resistance characteristics. Also, the Ti–*x*Hf alloy system does not form any intermetallic compounds, which is important for good corrosion resistance [13–15]. However, to the best of our knowledge there are only a few reported studies on the corrosion resistance of Ti–*x*Hf alloys. In fact, knowledge about the effect of Hf content on the corrosion resistance of Ti alloys is very limited [15].

The electrochemical anodization process provides an effective surface coating technology for titanium alloys because large-area coatings can be achieved with good mechanical adhesion. Since the thin titanium oxide surface film is chemically bonded to the titanium alloy substrate, the electrical conductivity of the specimen being anodized is good. However, the limited thickness of anodic pores in the TiO_2 layer must be adjusted by controlling the anodic

Y.-H. Jeong · H.-C. Choe (✉) · W. A. Brantley
Department of Dental Materials, Research Center of Nano-Interface Activation for Biomaterials, Chosun University, Gwangju, Korea
e-mail: hcchoe@chosun.ac.kr

Y.-H. Jeong · H.-C. Choe
Research Center for Oral Disease Regulation of the Aged School of Dentistry, Chosun University, Gwangju, Korea

W. A. Brantley
College of Dentistry, Ohio State University, Columbus, OH, USA

conditions [16–23]. Anodic oxidation of titanium has been widely used for surface modification of bio-implants because of many advantages. The fabrication of porous titanium oxide films through dielectric breakdown provides improved film adhesion to the substrate metal, and helps in achieving high-quality films by varying the electrolytes, temperature, alloying element, voltage, current density and time [24, 25]. Also, anodizing can be used to increase the oxide thickness to improve corrosion protection and to decrease ion release [26]. There has been one report on the corrosion behavior of anodized Ti–*x*Hf alloys [12], and this report suggested the present study of the corrosion of anodized Ti–Hf alloys.

This paper presents a study of the effect of anodizing on the corrosion behavior of Ti–*x*Hf alloys, using electrochemical methods.

2 Experimental

Four Ti–*x*Hf binary alloys, with Hf contents ranging from 10 to 40 wt% (in 10 wt. % increments) were prepared using CP titanium (G&S Titanium, Grade 4, USA) and hafnium (Kurt J. Lesker Company, 99.95 wt. % purity, USA). The Ti–*x*Hf alloys were prepared from the component metals, using a vacuum arc-melting furnace (SVT, Korea) with a water-cooled copper hearth and a high-purity argon atmosphere. The sponge Ti that formed was initially melted in a chamber which served as an oxygen scavenger to minimize the residual oxygen level before the weighed charges of Ti and Hf were subsequently melted to prepare each alloy ingot. The Ti–*x*Hf ingots were remelted at least six times in order to avoid inhomogeneity, and then homogenized in a furnace (Model MSTF-1650, MS Eng, Korea) for 24 h at 1000°C in an Ar atmosphere, followed by quenching in 0°C water.

Cylindrical specimens (diameter 10 mm, thickness 5 mm) were cut from cast ingots of the Ti–*x*Hf alloys, mechanically polished with 600 grit SiC and 1 μm Al_2O_3 slurry, degreased by ultrasonic cleaning in acetone, and dried in air. Platinum was polished similarly to serve as the counter electrode in an electrochemical cell. All anodization experiments were performed at room temperature in a standard glass cell. Pores were formed on the Ti–*x*Hf alloy surface by anodizing (KDP-1500 DC power supply, Korea) at potentials of 120, 170, and 220 V for 10 min. The electrolyte with 1.0 M H_3PO_4, which was prepared from reagent grade chemicals and distilled water, was stirred during anodization. Then, the anodized samples were rinsed in distilled water and acetone, and dried in air. Crystallization heat treatments of the anodized surfaces were performed in an Ar atmosphere at 300 and 500°C for 1 h.

The phases on the anodized surfaces were determined by an x-ray diffractometer (XRD, Philips, X'pert PRO) using Cu Kα radiation. The surface morphology was observed with a field emission scanning electron microscope (FE-SEM, Hitachi 4800, Japan).

The corrosion behavior of the Ti–*x*Hf alloys was investigated with a standard three-electrode cell having the alloy specimen as a working electrode and a high density carbon counter electrode. The potential of the working electrode was measured against a saturated calomel electrode (SCE), and all of the measured potentials were referenced to this electrode. The corrosion properties of the specimens were examined by the potentiodynamic polarization test method (potential range of −1500 to 2000 mV: SCE) at a scan rate of 1.67 mV/s in 0.15 M NaCl solution maintained at 36.5 ± 1°C (PARSTAT 2273, EG&G, USA). An initial conditioning treatment for each sample was performed cathodically at −1500 mV (SCE) for 10 min before the corrosion test. The corrosion data including the corrosion current density (I_{corr}) were obtained from the polarization curves using Tafel plots on the linear portion of the cathodic and anodic branches near zero current density.

3 Results and discussion

Figure 1 shows XRD patterns from the Ti–(10, 20, 30 and 40 wt%) Hf alloys after the heat treatment in an Ar atmosphere for 24 h at 1000°C. The peaks were identified using the JCPDS diffraction data for Ti and Hf powder

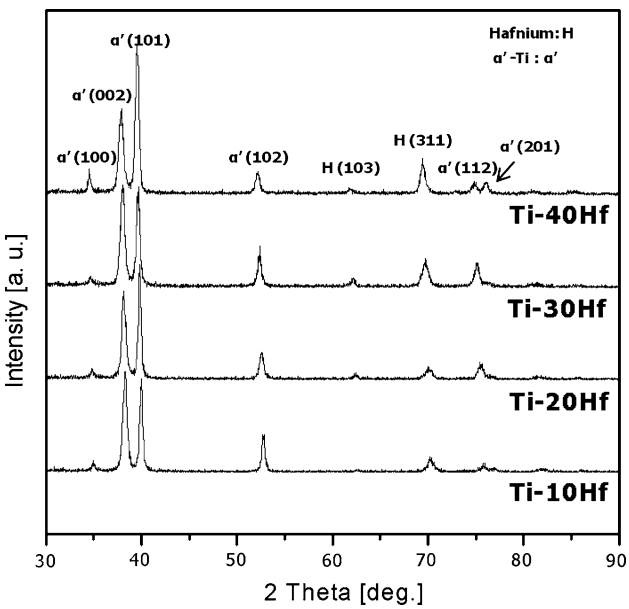

Fig. 1 XRD patterns for heat treated Ti–*x*Hf alloys in Ar atmosphere for 24 h at 1000°C

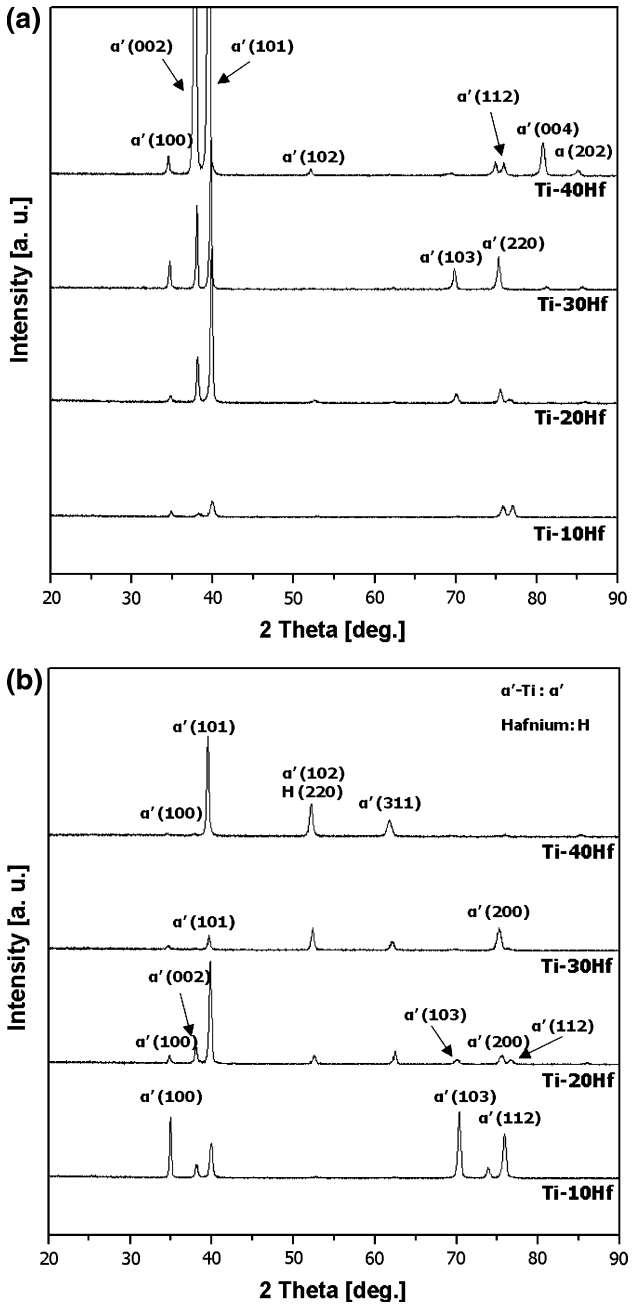

Fig. 2 XRD patterns of anodized Ti–*x*Hf alloys at 170 V (**a**) and 220 V (**b**)

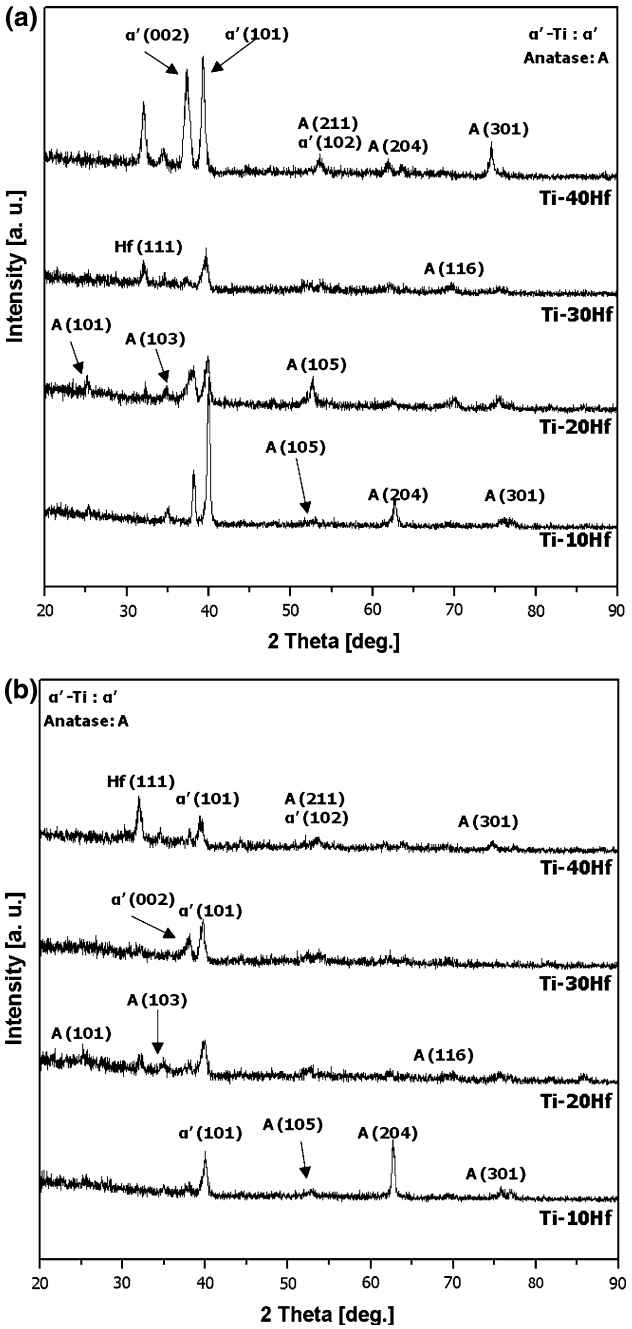

Fig. 3 XRD patterns of crystallized Ti–*x*Hf alloys at 300°C after anodizing at 170 V (**a**) and 220 V (**b**)

standards. It can be seen that the principal reflections occurred from the (002) and (101) atomic planes from α'-Ti at 2θ values of 38.48 and 40.17°, respectively. Peaks from the hafnium solid solution phase were also present, and became more prominent with increasing Hf content. It has been reported that Ti–Hf alloys undergo phase transformation resulting in the formation of an hcp phase [12, 15, 27].

Figures 2, 3, and 4 summarize the XRD results for the Ti–*x*Hf alloys after anodization at different applied voltages and heat treatment (crystallization) temperatures. Figure 2a, b present XRD patterns from the Ti–*x*Hf alloys anodized at 170 and 220 V, respectively. Only α'-Ti peaks were observed for all the samples, and no TiO_2 anatase peaks were present because of the amorphous oxide structure on the anodized surfaces. Figure 3a, b show the XRD patterns from the Ti–*x*Hf alloys anodized at 170 and 220 V, respectively, followed by crystallization heat treatment in an Ar atmosphere for 6 h at 300°C. Figure 4a,

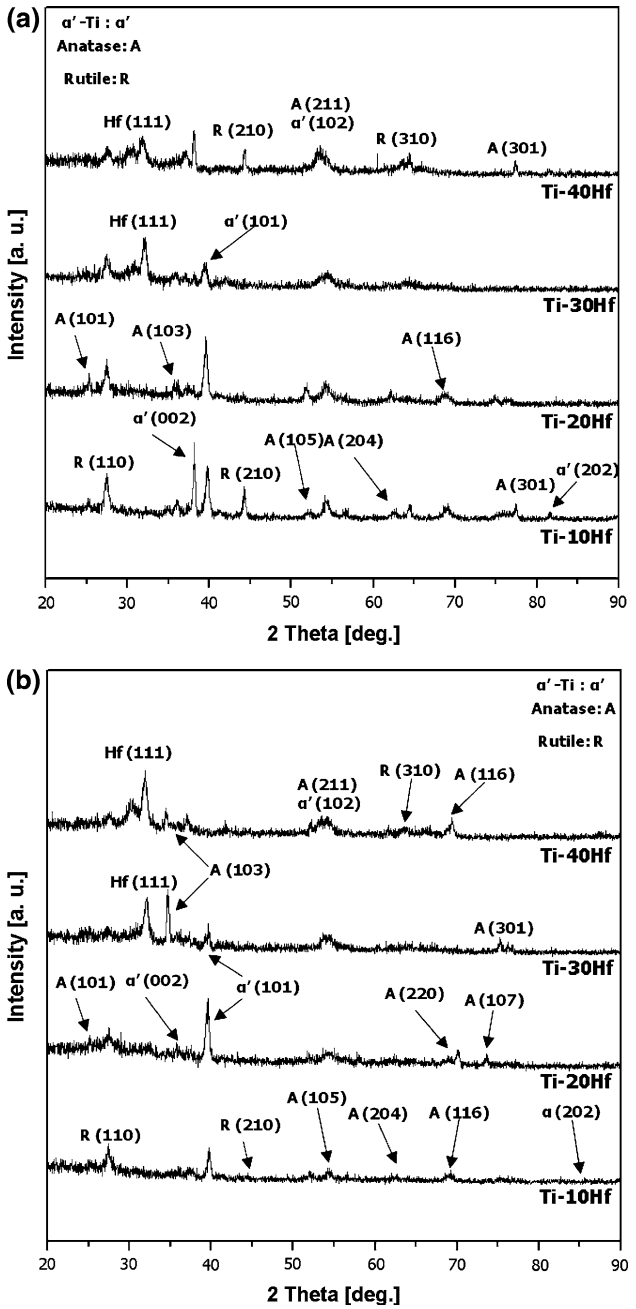

Fig. 4 XRD patterns of crystallized Ti–*x*Hf alloys at 500°C after anodizing at 170 V (**a**) and 220 V (**b**)

b shows the XRD patterns from the Ti–*x*Hf alloys anodized at 170 and 220 V, respectively, followed by crystallization heat treatment in an Ar atmosphere for 6 h at 500°C. The α′-Ti phase, Hf solid solution and anatase form of TiO_2 are evident in Figs. 3a, and 4a. In contrast, the α′-Ti phase, Hf solid solution phase, anatase and the rutile form of TiO_2 can been seen in Figs. 3b, 4b, respectively. The α′-Ti peaks from the crystallized samples in Figs. 3a, b and 4a, b had lower intensity than those from the amorphous oxide samples in Fig. 2a, b. The rutile TiO_2 peaks were detected in the crystallized samples shown in Fig. 4a, b that had been heat treated in an Ar atmosphere at 500°C following anodization. The intensities of the α′-Ti peaks were decreased with higher anodization voltage and subsequent heat treatment (crystallization) temperature. Moreover, the crystallized samples exhibited predominantly anatase peaks. It is well known that TiO_2 has three crystal structures; anatase, rutile and brookite. The anatase form is considered to be superior for biomedical applications because of a more reactive nature compared to rutile and brookite [28], and it can be formed preferentially by anodization under the appropriate conditions of applied potential and crystallization heat treatment [28].

Figure 5 shows the microstructures of the Ti–(10, 20, 30 and 40 wt%) Hf alloys after homogenization heat treatment at 1000°C for 24 h in an Ar atmosphere followed by quenching in water at 0°C. All of these samples had a martensitic type of structure. The structures of the Ti–10Hf and Ti–20Hf alloys were more of the lamellar type, while the Ti–30Hf had complex microstructure consisting of both lamellar and needle-like constituents. The Ti–40Hf alloy had a fine needle-like microstructure without the broader lamellae. It was evident that the lamellar microstructure was altered to a needle-like microstructure with increasing Hf content.

Figure 6 shows FE-SEM images of the anodized surfaces of the Ti–*x*Hf alloys, and in particular the effects of the anodizing voltage in creating surface porosity. The anodization process caused porous surfaces to form on the Ti–*x*Hf alloys in 1.0 M H_3PO_4 solution when constant cell voltages of 120, 170 and 220 V were applied for 10 min. The pore sizes ranged from approximately 300 nm to 1 μm, and the homogeneity of the pore distribution across the titanium alloy surface was found to depend on the Hf content and anodizing voltage. The samples anodized at 120 V exhibited less surface porosity when compared to the samples anodized at 170 and 220 V. However, the Ti–40Hf alloy anodized at 120 V formed a nonporous surface film. For all of the Ti–Hf alloys, the pore size was dependent on the anodizing voltage. The Ti–10Hf and Ti–20Hf alloys exhibited the most homogeneous porous structures. Higher contents of Hf in the titanium alloys resulted in a nonuniform porous structure with fewer pores. In particular, for the Ti–40Hf alloy anodized at 220 V, the largest porous structures had a crater-like appearance and were formed in a relatively small area, presumably because Hf has excellent corrosion resistance when alloyed with Ti [12, 13, 15, 28]. It was conjectured that a spark discharge process acted to create a higher current density on the surface of the Ti–40Hf alloy during the anodizing process than occurred for anodizing of the Ti–10, 20, and 30Hf alloys [28]. Therefore, for the Ti–10Hf and Ti–20Hf alloys, homogeneous porous structures were easily formed on the

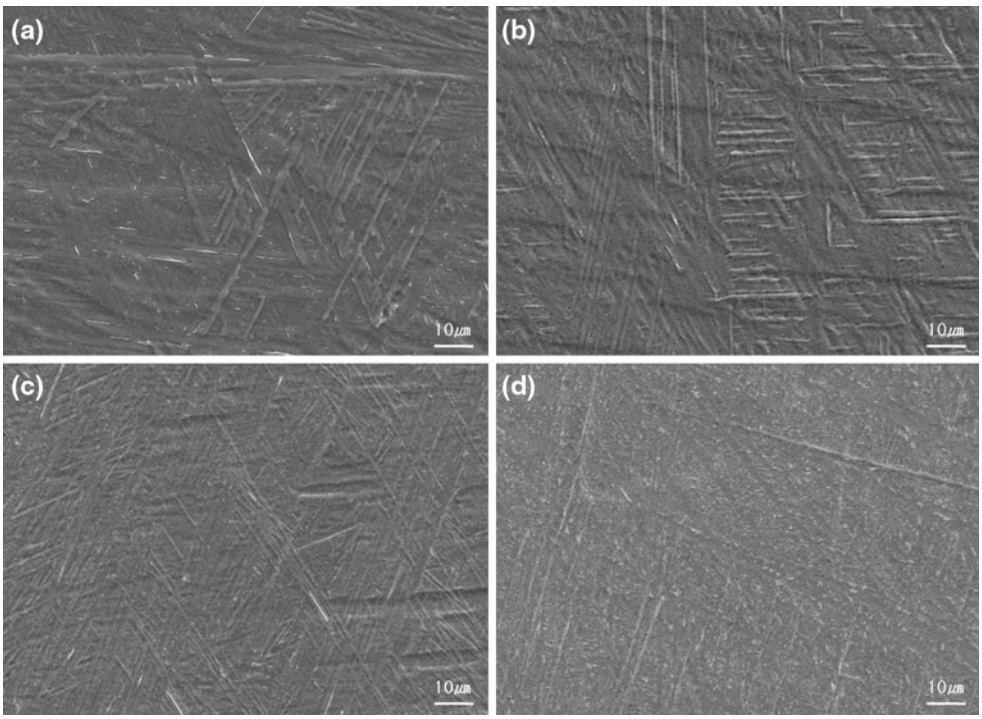

Fig. 5 FE-SEM images of Ti–*x*Hf alloys after heat treatment at 1000°C for 24 h in Ar atmosphere, followed by 0°C water quenching: **a** Ti–10Hf; **b** Ti–20Hf; **c** Ti–30Hf; and **d** Ti–40Hf

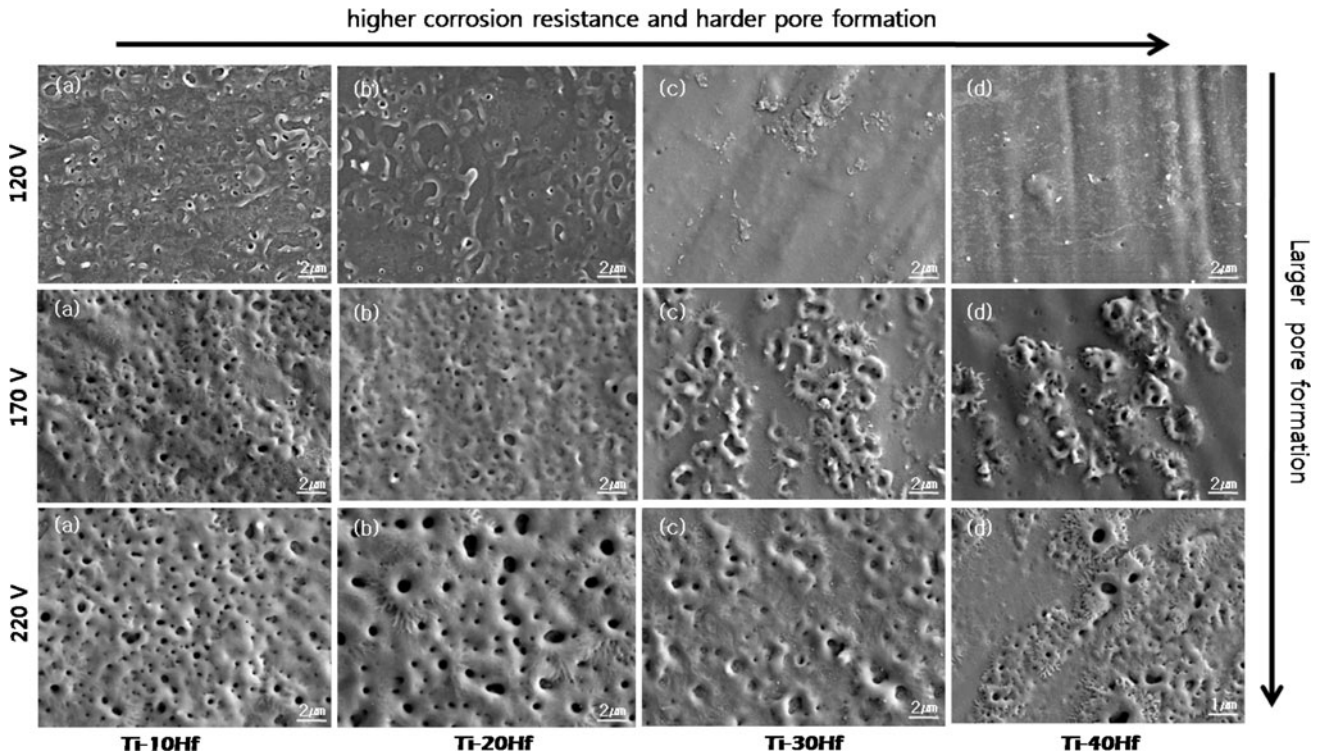

Fig. 6 FE-SEM images of Ti–*x*Hf alloys with varying applied voltage (120, 170, and 220 V) and Hf content (10, 20, 30, and 40 wt%): **a** Ti–10Hf; **b** Ti–20Hf; **c** Ti–30Hf; and **d** Ti–40Hf

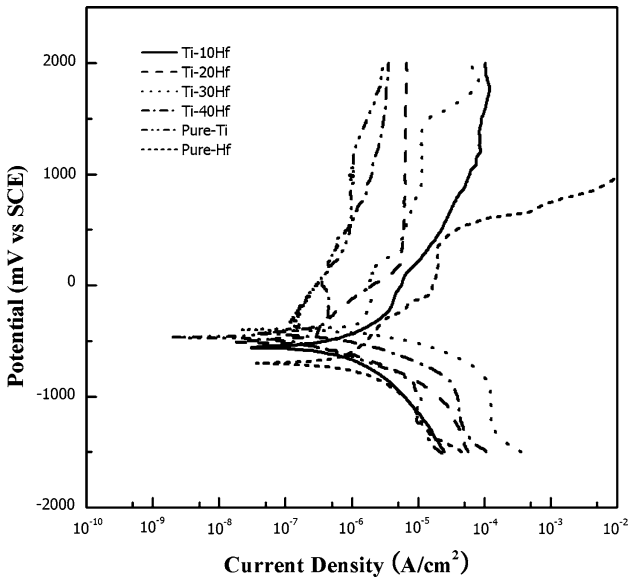

Fig. 7 Anodic polarization curves of Ti–*x*Hf alloys, pure Ti and pure Hf after potentiodynamic testing in 0.15 M NaCl solution at 36.5 ± 1°C

anodized surface when compared to the Ti–30Hf and Ti–40Hf alloys.

Figure 7 shows the potentiodynamic polarization curves for pure Ti, pure Hf, and the Ti–*x*Hf alloys in 0.15 M NaCl solution at 36.5 ± 1°C. The corrosion potentials (E_{corr}) of pure Ti and pure Hf were −467 mV (SCE) and −700 mV (SCE), respectively, and the corrosion current densities (I_{corr}) of pure Ti and Hf were 1.15×10^{-7} and 1.94×10^{-6} A/cm^2, respectively. From the polarization curves, pure Ti has superior corrosion resistance compared to pure Hf. Pitting corrosion behavior was observed in the anodic polarization curve of pure Hf at 500 mV (SCE). It is thought that HfO_2 film was easily broken down by Cl^- ions at the site of surface defects such as scratches, grooves, and ridges [15], as well as the needle-like structure shown in Fig. 5. The anodic polarization curves were shifted to the left and upward with increasing Hf content in the Ti–*x*Hf alloys. The values of E_{corr} for the Ti–10Hf and Ti–40Hf alloys were −560 mV (SCE) and −430 mV (SCE), respectively, and the values of I_{corr} for Ti–10Hf and Ti–40Hf alloys were 1.10×10^{-7} and 2.89×10^{-7} A/cm^2, respectively. The Ti–*x*Hf alloys had good corrosion resistance, and pitting corrosion behavior was not apparent in the anodic polarization curves of the Ti–*x*Hf alloys. Thus Hf can contribute to the corrosion resistance when it is alloyed with Ti, since the Ti–*x*Hf alloys form isomorphous systems. The absence of intermetallic compounds in these alloys enhance their corrosion resistance [12, 13]. As a result, the highest corrosion potential and stable passive region of the Ti–40Hf alloy are attributed to the incorporation of Hf providing excellent corrosion resistance. The observation that Ti–*x*Hf alloys exhibit better corrosion resistance than pure Ti and pure Hf suggests that the passive film containing a mixture of TiO_2 and HfO_2 is more stable and stronger than the passive films of TiO_2 and HfO_2 that form on pure Ti and pure Hf [15]. Pure hafnium is used in the nuclear industry because of its superior corrosion resistance, and Hf undergoes nodular corrosion to form HfO_2 [12, 13].

It is well known that the corrosion resistance of metals and alloys is greatly influenced by the electrolyte composition, temperature, microstructure, and alloying elements [29]. In the present study, there are no pronounced differences in the microstructures of Ti–*x*Hf alloys, but the improvement in corrosion resistance of Ti–*x*Hf alloys is confirmed to be a function of Hf content. For the potential found in the oral environment (at 300 mV), the current densities of the Ti–10Hf and Ti–40Hf alloys were 1.32×10^{-5} and 5.56×10^{-7} A/cm^2, respectively. The present results show that the Ti–40Hf alloy exhibit superior corrosion resistance compared to the Ti–10Hf alloy. From Fig. 7, it can be seen that the Ti–40Hf alloy had higher values of E_{corr} and lower values of I_{corr}, compared to the other Ti–Hf alloys in the 0.15 M NaCl solution. The Ti–*x*Hf alloys were characterized by wide passive regions with nearly constant values of passive current density, indicating that their corrosion rates were in steady state and that the passive films formed on their surfaces were stable [15]. The passive current density for the Ti–40Hf alloy was lower than that for the Ti–10Hf alloy in the 0.15 M NaCl solution. Moreover, at the potential of the oral environment, all of the Ti–*x*Hf alloys exhibited very stable passive film formation. The passivation regions of the Ti–*x*Hf alloys presented higher values of current density with inceasing Hf content.

Figures 8, 9, and 10 show the polarization curves in the 0.15 M NaCl solution at 36.5 ± 1°C for the Ti–*x*Hf alloys anodized in 1.0 M H_3PO_4 solution at cell voltages of 120, 170, and 220 V for 10 min, respectively. It was found that the anodic polarization curves were shifted to the left with increasing anodizing voltage. The values of E_{corr} for Ti–10Hf and Ti–40Hf anodized at 120 V was −560 mV (SCE) and −410 mV (SCE), respectively, whereas the corresponding values of I_{corr} for these alloys anodized at 120 V was 7.23×10^{-7} and 1.94×10^{-7} A/cm^2, respectively. It was found that the anodized Ti–*x*Hf alloys had superior corrosion resistance compared to the non-anodized alloys.

The current density in the transpassive region (about 1000 mV) was increased due to the oxygen evolution reaction ($2H_2O \rightarrow O_2 + 4H^+ + 4e^-$ or $4OH^- \rightarrow O_2 + 2H_2O + 4e^-$) on the microporous surface as shown in Fig. 8. Additionally, the micropores were attacked by Cl^- ions in the electrolyte. The chloride solution strongly promotes the anodic dissolution in the micropores formed on TiO_2, and

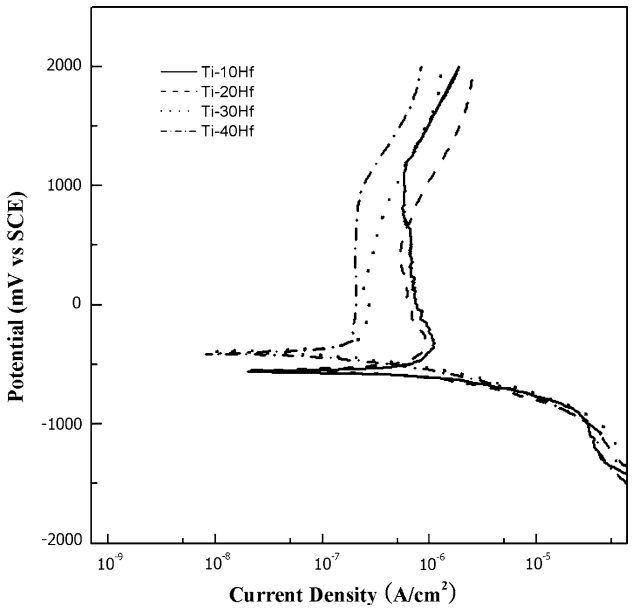

Fig. 8 Anodic polarization curves of Ti–*x*Hf alloys anodized at 120 V after potentiodynamic testing in 0.15 M NaCl solution at 36.5 ± 1°C

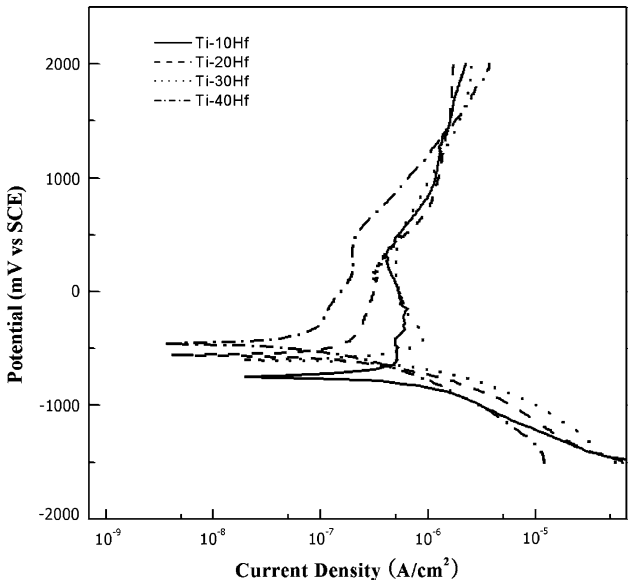

Fig. 9 Anodic polarization curves of Ti–*x*Hf alloys anodized at 170 V after potentiodynamic testing in 0.15 M NaCl solution at 36.5 ± 1°C

thus the transpassive potential decreased with anodization potential for the Ti–*x*Hf alloys due to the resulting large pores. The Cl^- ions can migrate into the pores and across the passive oxide film in parallel with the oxide ions. When the chloride ions reach the metal-passive film interface, the metal chloride is formed. Metal chlorides play a major role in the fracture of oxide films depending on the amount of accumulated metal chloride [15].

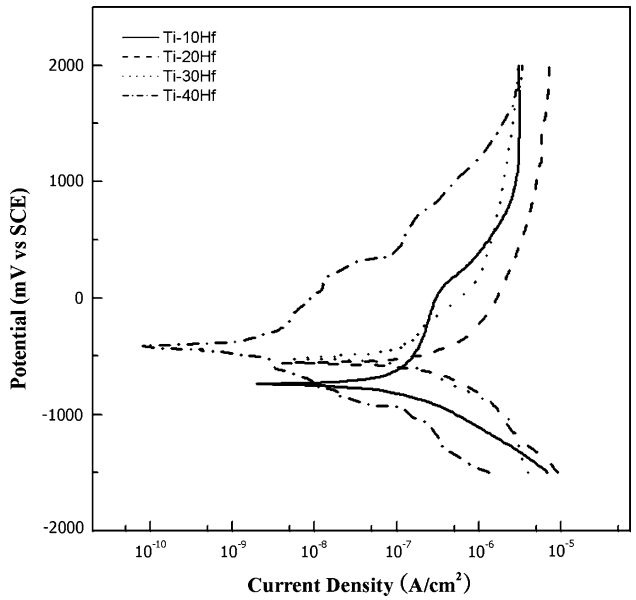

Fig. 10 Anodic polarization curves of Ti–*x*Hf alloys anodized at 220 V after potentiodynamic testing in 0.15 M NaCl solution at 36.5 ± 1°C

It is evident that the anodized Ti–*x*Hf alloys have lower I_{corr} and higher E_{corr} than those of the non-anodized Ti–*x*Hf alloys. The anodized Ti–*x*Hf alloys had good in vitro corrosion resistance (higher E_{corr} and lower I_{corr}), which improved with increasing anodized voltage. The anodized Ti–40Hf alloy has the highest value of E_{corr} and the lowest value of I_{corr} compared to the other Ti–*x*Hf alloys, and the Ti–40Hf alloy anodized at 220 V had the highest corrosion resistance. It was thought that the Ti–*x*Hf alloys anodized at 220 V had thicker oxide layers than the Ti–*x*Hf alloys anodized at 120 and 170 V. The increase in corrosion resistance for these binary titanium alloys with increasing Hf content is attributed to the thick passive film, such as TiO_2 and HfO_2, formed on the alloy surface by the anodizing treatment. A thick passive film should restrict the movement of metal ions from the metal surface to the solution and thus minimize corrosion of the Ti–*x*Hf alloy [29–31].

Table 1 shows the transpassive and pitting potentials measured from the anodic polarization tests for the anodized Ti–*x*Hf alloys. As shown in Table 1, all of anodized Ti–*x*Hf alloys had pitting potentials. The transpassive potential (E_{trans}) of anodized Ti–10Hf at 120 V anodizing voltage was about 1070 mV (SCE), whereas E_{trans} at 170 V was about 290 mV and about 40 mV (SCE) at 220 V. The value of E_{trans} for anodized Ti–40Hf at 120 V was about 930 mV (SCE), whereas E_{trans} at 170 V was about 510 mV and E_{trans} at 220 V was about 320 mV (SCE). With increasing amount of Hf, there was an increase in the transpassive potential of the Ti–*x*Hf alloy. The addition of

Table 1 Values of corrosion potential (E_{corr} vs. SCE), pitting potential (E_{pit} vs. SCE), corrosion current density (I_{corr}) and current density I_{300} at 300 mV (potential of oral environment), obtained from potentiodynamic polarization curves of Ti–*x*Hf alloys, pure Ti, pure Hf and anodized Ti–*x*Hf alloys by applying voltage in 0.15 M NaCl solution at 36.5 ± 1°C

	Property	Ti–10Hf	Ti–20Hf	Ti–30Hf	Ti–40Hf	Pure Ti	Pure Hf
Non treatment	E_{corr} (mV)	−560	−500	−400	−430	−467	−700
	E_{trans}(mV)	–	–	–	–	–	–
	E_{pit} (mV)	–	–	–	–	–	500
	βa (mV/dec)	612.3	522.9	170	628.2	1018.6	1486.0
	βc (mV/dec)	565.9	221.5	1144	119.1	182.3	479.2
	I_{corr} (A/cm^2)	1.10×10^{-6}	2.43×10^{-7}	1.84×10^{-6}	2.89×10^{-7}	1.15×10^{-7}	1.94×10^{-6}
	I_{300} (A/cm^2)	1.32×10^{-5}	5.99×10^{-6}	5.0×10^{-6}	5.56×10^{-7}	7.22×10^{-7}	1.96×10^{-5}
120 V anodized	E_{corr} (mV)	−560	−550	−390	−410	–	–
	E_{trans} (mV)	1070	–	–	930	–	–
	E_{pit} (mV)	–	–	–	–	–	–
	βa (mV/dec)	335.0	534.2	856.4	831.0	–	–
	βc (mV/dec)	138.0	162.4	222.1	191.3	–	–
	I_{corr} (A/cm^2)	7.23×10^{-7}	5.27×10^{-7}	2.39×10^{-7}	1.94×10^{-7}	–	–
	I_{300} (A/cm^2)	6.76×10^{-7}	5.50×10^{-7}	2.80×10^{-7}	1.90×10^{-7}	–	–
170 V anodized	E_{corr} (mV)	−750	−560	−600	−460	–	–
	E_{trans} (mV)	–	–	–	–	–	–
	E_{pit} (mV)	290	450	500	510	–	–
	βa (mV/dec)	601.8	1322.1	1133.0	2412.6	–	–
	βc (mV/dec)	187.9	193.8	307.1	261.1	–	–
	I_{corr} (A/cm^2)	3.95×10^{-7}	1.85×10^{-7}	9.34×10^{-7}	1.12×10^{-7}	–	–
	I_{300} (A/cm^2)	8.24×10^{-7}	3.96×10^{-7}	5.00×10^{-7}	1.97×10^{-7}	–	–
220 V anodized	E_{corr} (mV)	−740	−560	−520	−410	–	–
	E_{trans} (mV)	–	–	–	–	–	–
	E_{pit} (mV)	40	–	–	320		
	βa (mV/dec)	2631.4	755.4	1114.1	632.4	–	–
	βc (mV/dec)	459.1	573.4	416.8	497.8	–	–
	I_{corr} (A/cm^2)	1.84×10^{-7}	4.46×10^{-7}	1.79×10^{-7}	2.12×10^{-9}	–	–
	I_{300} (A/cm^2)	7.78×10^{-7}	2.59×10^{-6}	1.15×10^{-6}	2.05×10^{-8}	–	–

Hf accelerated the formation of the passive film, which provided protection against attack by the Cl^- ions and resulted in increased corrosion resistance. In contrast, as the anodizing voltage increased, the transpassive potential also decreased. It was considered that the large pore formation occurring on the anodized surfaces resulted in lower corrosion resistance and led to greater surface attack by the Cl^- ions as shown in Fig. 6.

The mean values of corrosion potential (E_{corr} vs. SCE), transpassive potential (E_{trans} vs. SCE), pitting potential (E_{pit} vs. SCE), corrosion current density (I_{corr}), anodic Tafel slope (β_a), cathodic Tafel slope (β_c), and current density at 300 mV (the potential of oral environment) that were obtained from the polarization curves such as those shown in Figs. 7, 8, 9, and 10 are summarized in Table 1. The Tafel extrapolations on the polarization curves are commonly used for the measurement of corrosion current density. If the cathodic Tafel slope is extrapolated to the corrosion point, the corrosion rate, i.e., the corrosion current density (I_{corr}), can be obtained by the mixed potential theory. Then the β_a and β_c constants of the polarization resistance (R_p), which can be the key factor for calculating I_{corr}, can also be obtained. [32]. For the extrapolation process, the straight line for I_{corr} should be over an order of magnitude for current density to ensure accuracy.

However, in this study, it was very difficult to get the corrosion current density because there is only a small linear region in the anodic portion of the polarization plot due to the formation of dense passive surface oxides by the anodization process. Nevertheless, reasonable estimates of corrosion current density are possible despite the limited Tafel behavior, and the values of corrosion current density (I_{corr}) could be determined from the point of intersection between the corrosion potential line and the cathodic

branch of the polarization curve. To obtain the steady state polarization curve, which shows the correct corrosion reaction, the potentiodynamic polarization tests were only performed when the open circuit potential showed a constant value with time.

From this study, we have presented evidence that the anodized Ti–*x*Hf alloys having high corrosion resistance and porous surface morphology are suitable for biomedical applications.

4 Conclusions

All of the anodized Ti–*x*Hf alloys exhibited XRD peaks for the α'-phase of Ti, while no peaks of the anatase form of TiO_2 were detected. After a crystallization heat treatment at 300°C, the surfaces of the Ti–*x*Hf alloys were composed of α'-Ti and anatase phases. When the anodized Ti–*x*Hf alloys were subjected to crystallization heat treatment at 500°C, their surfaces were composed of both the anatase and rutile forms of TiO_2. The relative amount of α'-Ti observed in the XRD patterns decreased as the applied voltage and crystallization temperature increased. The XRD peaks of anatase and rutile that appeared after crystallization heat treatment for the anodized specimen appeared predominantly with decreasing Hf contents for the binary Ti–*x*Hf alloys.

Microstructural observations revealed that the surfaces of the anodized Ti–10Hf and Ti–20Hf alloys contained more pores compared to the Ti–30Hf and Ti–40Hf alloys. For the non-anodized Ti–*x*Hf alloys, the lamellar microstructure was transformed to a needle-like microstructure with increased Hf content. For the anodized Ti–*x*Hf alloys, pores with sizes ranging from approximately 300 nm to 1 μm were distributed over the surfaces, with their homogeneity depending on the Hf content and anodizing voltage. The pore diameter increased with the applied voltage for anodizing, and the most regular array of larger diameter pores was formed on the Ti–20Hf alloy anodized at 220 V.

The potentiodynamic polarization test results showed that the anodized Ti–*x*Hf alloys have lower corrosion current density (I_{corr}) and higher corrosion potential (E_{corr}) than the non-anodized Ti–*x*Hf alloys. The anodized Ti–40Hf alloy had the highest corrosion potential (E_{corr}) and lowest corrosion current density (I_{corr}), which is attributed to the excellent corrosion resistance resulting from the presence of hafnium. The transpassive potential of the anodized Ti–*x*Hf alloys increased with the Hf content, and as the anodizing voltage increased, the transpassive potential decreased.

Acknowledgments This research was supported by National Research Foundation of Korea (R13-2008-010-00000-0).

References

1. Rao S, Ushida T, Tateishi T, Okazaki Y, Asao S. Effect of Ti, Al and V ions on the relative growth rate of fibroblasts (L929) and osteoblast (MT3T3-E1) cells. J Biomed Mater Eng. 1996;6:79–86.
2. Kobayashi E, Gardner LK, Toth RW J. Titanium: the mystery metal of implant dentistry. Dental materials aspects. J Prosthet Dent. 1985;54:410–4.
3. He G, Hagiwara M. Ti alloy design strategy for biomedical applications. Mater Sci Eng. 2006;C26:14–9.
4. Steinemann SG. In: Winter GD, Leray JL, de Groot K, editors. Evaluation of biomaterials. New York: John Wiley & Sons Ltd; 1980. p. 1–34.
5. McLachlan C, Farnell B, Galin H. In: Sarkar B, editor. Biological aspects of metals and metal-related diseases. New York: Raven Press; 1983. p. 209–18.
6. Perl DP, Brody AR. X-ray spectrometric evidence of aluminum accumulation in neurofibrillary tangle-bearing neurons. Science. 1980;208:297–9.
7. Sumner DR, Galante JO. Determinants of stress shielding: design versus materials versus interface. Clin Orthop Relat Res. 1992;274:202–12.
8. Niinomi M. Recent metallic materials for biomedical applications. Metall Mater Trans. 2002;33:477–86.
9. Niinomi M. Mechanical properties of biomedical titanium alloys. Mater Sci Eng. 1998;A243:231–6.
10. Long M, Rack HJ. Titanium alloys in total joint replacement-a materials science perspective. Biomater. 1998;19:1621–39.
11. Saji VS, Choe HC. Electrochemical corrosion behaviour of nanotubular Ti–13Nb–13Zr alloy in Ringer's solution. Corros Sci. 2009;51:1658–63.
12. Jeong YH, Kim WG, Park GH, Choe HC, Ko YM. Surface characteristics of HA coated Ti–Hf binary alloys after nanotube formation. Trans Nonferr Metals Soc China. 2009;19:852–6.
13. Cai Z, Koike M, Sato H, Brezner M, Guo Q, Komatsu M, Okuno O, Okabe T. Electrochemical characterization of cast Ti–Hf binary alloys. Acta Biomater. 2005;1:353–6.
14. Jeong YH, Lee K, Choe HC, Ko YM, Brantley WA. Nanotube formation and morphology change of Ti alloys containing Hf for dental materials use. Thin Solid Films. 2009;517:5365–9.
15. Zhou YL, Niinomi M. Passive films and corrosion resistance of Ti–Hf alloys in 5% HCl solution. Surf Coat Technol. 2009;204:180–6.
16. Kubota S, Johkura K, Asanuma K, Okouchi Y, Ogiwara N, Sasaki K, Kasuga T. Titanium oxide nanotubes for bone regeneration. J Mater Sci Mater Med. 2004;15(9):1031–5.
17. Kakoli D, Susmita B, Amit B. Surface modifications and cell-materials interactions with anodized Ti. Acta Biomater. 2007;3:573–85.
18. Limmer SJ, Chou TP, Cao GZ. A study on the growth of TiO_2 nanorods using sol electrophoresis. J Mater Sci. 2004;39:895–901.
19. Kim WG, Choe HC, Ko YM, Brantley WA. Nanotube morphology changes for Ti–Zr alloys as Zr content increases. Thin Solid Films. 2009;517(17):5033–7.
20. Jang SH, Choe HC, Ko YM, Brantley WA. Electrochemical characteristics of nanotubes formed on Ti–Nb alloys. Thin Solid Films. 2009;517:5038–43.
21. Saji VS, Choe HC, Brantley WA. Nanotubular oxide layer formation on Ti–13Nb–13Zr alloy as a function of applied potential. J Mater Sci. 2009;44:3975–82.
22. Saji VS, Choe HC. Phenomena of nanotube nucleation and growth on new ternary titanium alloys. Acta Biomater. 2009;5:2303–10.

23. Bai J, Zhou B, Li L, Liu Y, Zheng Q, Shao J, Zhu X, Cai W, Liao J, Zou L. J Mater Sci. 2008;43:1880–4.
24. Zwilling V, Aucouturier M, Darque-Ceretti E. Anodic oxidation of titanium and TA6V alloy in chromic media. An electrochemical approach. Electrochim Acta. 1999;45:921–9.
25. Jakubowicz J. Formation of porous TiO_x biomaterials in H_3PO_4 electrolytes. Electrochem Commun. 2008;10:735–9.
26. Song HJ, Kim MK, Jung GC, Vang MS, Park YJ. The effects of spark anodizing treatment of pure titanium metals and titanium alloys on corrosion characteristics. Surf Coat Technol. 2007;201:8738–45.
27. Zhou YL, Niinomi M, Akahori T. Changes in mechanical properties of Ti alloys in relation to alloying additions of Ta and Hf. Mater Sci Eng. 2008;A483:153–6.
28. Oh HJ, Lee JH, Jeong YS, Kim YJ, Chi CS. Microstructural characterization of biomedical titanium oxide film fabricated by electrochemical method. Surf Coat Technol. 2005;198:247–52.
29. Choe HC, Kim HS, Choi DC, Kim KH. Effects of alloying elements on the electrochemical characteristics of iron aluminides. J Mater Sci. 1997;32:1221–7.
30. Choe HC, Jeong YH, Brantley WA. Phenomena of nanotube nucleation and growth on new ternary titanium alloys. J Nanosci Nanotech. 2010;10:4684–9.
31. Narayanan R, Seshadri SK. Phosphoric acid anodization of Ti–6Al–4V—structural and corrosion aspects. Corros Sci. 2007;49:542–58.
32. Mansfeld F. Advances in corrosion science and technology. In Fontana MG, Staehle RW, editors. 6th ed. Plenum Press: New York; 1976.